Journal of Volcanology and Geothermal Research 196 (2010) 236–244

Contents lists available at ScienceDirect

Journal of Volcanology and Geothermal Research

journal homepage: www.elsevier.com/locate/jvolgeores

Pressures at the base of dry flows of angular rock fragments as a function of grain size and flow volume: Experimental results

B. Cagnoli [a,*], G.P. Romano [b]

[a] Istituto Nazionale di Geofisica e Vulcanologia, Via di Vigna Murata 605, 00143 Rome, Italy
[b] Department of Mechanics and Aeronautics, La Sapienza University, Via Eudossiana 18, 00184 Rome, Italy

ARTICLE INFO

Article history:
Received 16 March 2010
Accepted 2 August 2010
Available online 10 August 2010

Keywords:
pyroclastic flows
rock avalanches
angular rock fragments
basal pressure
mobility

ABSTRACT

Geophysical granular flows such as pyroclastic flows and rock avalanches kill people and damage properties worldwide. The pressures exerted at their base affect the retarding forces that act on them and, for this reason, affect also their mobility that is important to foresee when assessing natural hazards in mountain regions. Here we present the results of experiments obtained by measuring with a load cell the basal pressures exerted by dry and cohesionless granular flows that descend a curved chute in the laboratory. The interaction between these flows and the chute surface on which they travel is dominated by collisions of particles (and or clusters of particles). A dimensional analysis suggests that the energy dissipation of these flows increases as grain size increases and as flow volume decreases (all the other features equal). Therefore the smaller the grain size and the larger the volume, the larger is expected to be flow mobility. Although, the longer travel distances of the centre of mass of finer grain size flows are easily discernible in our experiments, the effect of volume is probably hidden by additional phenomena such as the deposition first of the frontal portion of longer flows on the less-steep more-distal part of the slope that prevents the rear portion and the centre of mass of the flows to travel further downhill.

1. Introduction

This paper focuses on the effects that grain size and flow volume have on the basal pressure exerted by dry flows of angular rock fragments that descend a curved chute in the laboratory. Examples in nature of these flows are pyroclastic flows and rock avalanches that are considered among the most hazardous natural phenomena (Schmincke, 2004; Pudasaini and Hutter, 2006). Basal pressure plays a key role in their mobility because it affects the retarding force that acts on them. In geophysical flow modelling, this retarding force is often estimated using Coulomb's law where the frictional stress is equal to the normal stress multiplied by a coefficient of friction (Savage and Hutter, 1989; Sheridan et al., 2005; Mangeney et al., 2007).

The results described here are consistent with an interaction between flows and ground dominated by collisions. The main difference between our data and those obtained by other authors is that our load cell signal is equal to zero from time to time during flow transit between what we interpret to be collisions. In other experiments (e.g., Bartelt et al., 2007) the signal recorded between flow front and flow rear tip is always different from zero. This difference is due to different ratios between the diameter of the load cell plate and the size of the fragments. In the case of Bartelt et al. (2007), for example, the plate is 264 cm^2 and the grain size is 75–150 μm so that there are always fragments in contact with their plate during the flow transit and their sensor measures the effect of all these fragments together. The resulting average stress values refer to the models which adopt, for example, Coulomb's law. In our experiments, on the other hand, the ratio between plate diameter (5 mm) and grain size (0.5–3 mm) is significantly smaller so that the load cell resolves the interactions of single rock fragments (or single clusters of fragments). This is important to understand how energy is dissipated by travelling flows of dry and cohesionless angular rock fragments.

The results for dry flows presented here are also expected to differ from those that can be obtained for debris flows (e.g., Berti et al., 2000; McArdell et al., 2007) which are characterised by the presence of interstitial water and mud. It is reasonable to think, for example, that interstitial mud can affect basal pressure damping rock fragments collisions. However, flow plugs can form also in some debris flows (Johnson and Rodine, 1984) and we believe that the presence or absence of plugs can significantly change flow mobility (Cagnoli and Romano, 2010).

The purpose of this paper is to identify the main variables that govern flow mobility. By means of a dimensional analysis we propose the relationship between energy dissipation and important flow features: volume, grain size and initial speed. These results are consistent with field and experimental observations (Scheidegger, 1973; Cagnoli and Romano, 2010).

* Corresponding author.
E-mail address: bruno.cagnoli@ingv.it (B. Cagnoli).

0377-0273/$ – see front matter © 2010 Elsevier B.V. All rights reserved.
doi:10.1016/j.jvolgeores.2010.08.002

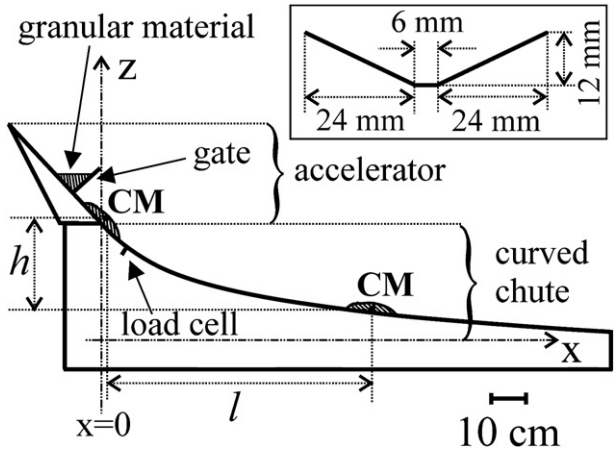

Fig. 1. Longitudinal cross-section of apparatus with location of load cell. Inset shows transversal cross-section of chute. CM stands for centre of mass.

2. Method

The experiments are carried out by releasing batches of angular rock fragments down a marble curved chute that is 5.4 cm wide and whose horizontal length is 1.4 m (Fig. 1). The chute is made of marble and it is placed on an extremely heavy table to prevent vibrations of the apparatus that can disturb the experiments. Before motion, the granular material rests behind a sliding gate on a metallic accelerating ramp (Fig. 1). The gate is opened manually. The shape of the chute is that of a hyperbolic sine equation:

$$z = 0.3 - 0.085 \operatorname{arcsinh}(11.765x). \quad (1)$$

This curve is a slightly modified version of the profile of Mayon Volcano in the Philippines (Becker, 1905). The chute has a trapezoidal transversal cross-section made of plaster whose asperities are significantly smaller than the smaller grain size we use. Both chute and accelerator have the same transversal cross-section (Fig. 1). There is no basal erosion in this apparatus because identical experiments carried out at earlier and later times do not show significantly different mobility due to a possible smoothing with time of the plaster surface. The experimental tests are run in a controlled environment where the average relative air humidity is approximately 42% at 25 °C.

The mixtures of angular rock fragments are obtained by crushing an aphanitic volcanic rock block and sieving the particles. Fragments density is ~2700 kg/m^3. The average angles of internal friction, obtained with seven bin-flow tests (Zenz and Othmer, 1960) for each grain size, are: $61.5 \pm 1°$, $62 \pm 1°$ and $60.5 \pm 1°$ for increasing grain size respectively (Cagnoli and Romano, 2010). These values are indistinguishable (because their error bars overlap) and they are relatively large as expected with angular rock fragments (Holtz and Kovacs, 1981). The angle of internal friction is affected by the angularity of the fragments and not, in general, by their grain size (Lambe and Whitman, 1969). It is important to realize that the angle of internal friction and the angle of basal friction have, in general, different values because they represent friction on different surfaces: an internal one and the ground surface respectively (Zenz and Othmer, 1960). The form, angularity and surface texture of our three grain sizes are not significantly different (Fig. 2). For this reason (and because these particles have the same angle of internal friction), we assume that the geometric properties of the three grain sizes are, as far as our results are concerned, indistinguishable.

A miniature load cell that measures normal forces is located on the chute (Fig. 1) at 10 cm from $x = 0$. In this location the slope angle is 36°. The sensitive plate of the load cell, which is 5 mm in diameter, is perfectly flush with the basal surface inside the chute. The load cell has been first tested to verify that its reaction to impulsive loading is identical to that obtained during the experiments. The travelling flows have been imaged by a high-speed video camera at 2000 fps (resolution: 1024×1024 pixels). The high-speed movies enable estimates of the initial speeds s of the flows (Table 2). We adopt as the initial speed that of the central part of the flows (where the centre of mass is located) when at $x = 0$ (Fig. 1). The field of view of the video camera is focused on the initial portion of the chute so that more details are visible in the images and the individual particles can be resolved.

Batches of granular material with two different masses (5 and 30 g) and three different grain size ranges (0.5–1, 1–2 and 2–3 mm) are used in the experiments with the load cell. Another set of experiments with the same three grain sizes but masses equal to 15 g has also been carried out without the load cell. Each experiment is repeated five times to assess its repeatability. In each test a different sample of granular material is used. No fine powder is produced by particles abrasion during flow motion.

3. Features of flows and deposits

During the initial deformation that occurs in the accelerator, the shape of the granular mass changes from that it has behind the gate into that of the slug-shaped travelling flows. Fig. 3 presents high-speed video camera images of the two travelling end-member flows with their mature shape of travel. The mature shape of travel is the shape the flows have during motion after the initial deformation in the accelerator (Fig. 1) and before the final deformation during deposition. Fig. 3A shows the end-member with larger volume and smaller grain size whereas Fig. 3B shows the end-member with smaller volume and larger grain size. The other flows plot in between as far as volumes and grain sizes are concerned.

The video camera confirms that all flows have already their mature shape of travel when they transit at $x = 0$ as well as when they transit on the load cell. This is important because the aim of this work is to measure the pressures at the base of travelling flows. The load cell is not located in a more distal position because it is already only a few centimetres away from the rear extremity of the 30 g deposits.

The deposited granular material consists of two portions: a more proximal elongated heap (the deposit of the flow proper) and a more distal distribution of individual fragments (Cagnoli and Romano, 2010). The average maximum thicknesses of the deposits are: 9, 7 and

Fig. 2. Photo of the angular rock fragments used in the experiments. The grain size increases from left to right (0.5–1, 1–2 and 2–3 mm, respectively).

Table 1
Mean pressure deviation ΔP (Pa) and mean pressure $\overline{P}$ (Pa) versus mean grain size (mm) and initial granular mass (g). The uncertainties are the error of the mean (i.e., the square root of the variance divided by the number of measurements).

	30 g		5 g	
	ΔP	$\overline{P}$	ΔP	$\overline{P}$
0.75 mm	155 ± 5 Pa	87 ± 4 Pa	82 ± 6 Pa	42 ± 3 Pa
1.5 mm	300 ± 23 Pa	95 ± 4 Pa	216 ± 10 Pa	53 ± 4 Pa
2.5 mm	535 ± 29 Pa	114 ± 4 Pa	437 ± 32 Pa	54 ± 4 Pa

4 mm for decreasing flow mass respectively. The distal distribution consists of fragments that, bouncing within the chute, travelled individually without interacting. Here we study only the flows considering that their movement and emplacement mechanisms differ substantially from those of the distal distribution of fragments. In our experiments there is no deposition of granular material on both sides of the travelling flows (i.e., there is no formation of levees).

Photos and laboratory measurements enable the determination of the position in space of selected points of the surfaces of the deposits (Cagnoli and Romano, 2010). Computer representations of these deposits are obtained joining these points with CAD software with which it is then possible to compute the position of the centres of mass. A similar procedure is adopted for the flows with the centre of mass at x = 0 on the chute (Fig. 1), where sideways high-speed video camera images enable estimates of the thicknesses of the flows. Here, we measure the distance between the centre of mass of the deposits and the flows centre of mass when at x = 0 on the chute (Fig. 1) to establish which flow is more mobile. We use the centre of mass at x = 0 instead of the centre of mass of the granular material at rest behind the gate because this second centre of mass cannot be compared with that of the deposits in the experiments with 15 and 5 g where the distal distribution of fragments is formed by a relatively too large a portion of the initial mass behind the gate. The initial centre of mass behind the gate can be used only with the 30 g flows (Cagnoli and Romano, 2010). For this reason, the initial granular mass does not enter the calculations.

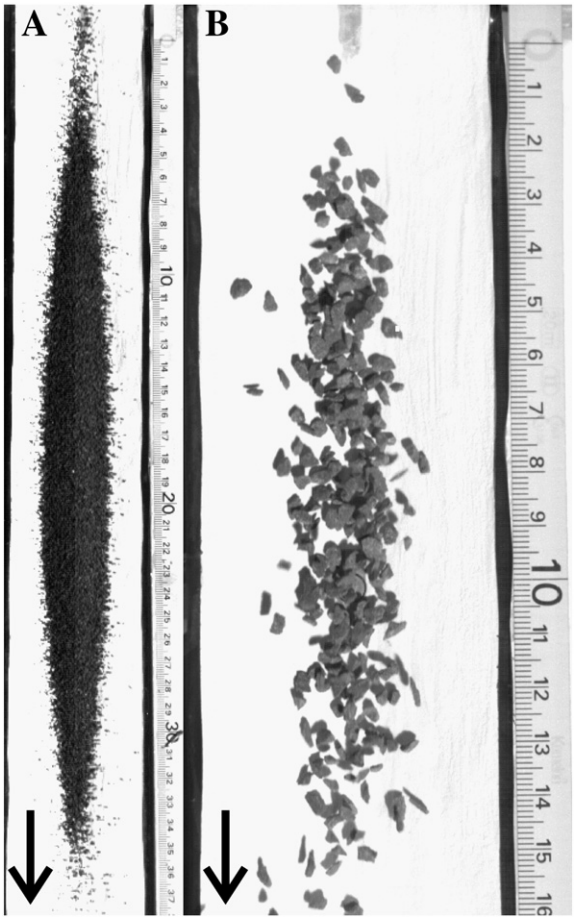

Fig. 3. Mature shape of travelling end-member flows. A) Flow with the largest volume and finest grain size. B) Flow with the smallest volume and coarsest grain size. The arrows show flow direction. The numbers in the tape measure are the centimetres from x = 0 (which is at the top of the chute). The gate is located 12.2 cm along the accelerator above x = 0.

4. Dimensionless parameters *D*, *n* and μ_A

The time-averaged pressure $\overline{P}$ exerted by each flow during all the time it is on the sensor is computed from the load cell data. This average takes into consideration also the zero-pressure data points between collisions so that this mean value of an intermittent pressure is suitable for comparison with the basal pressure of a sliding rigid body whose basal normal force is exerted continuously in time on the slope surface. We then calculate the average pressure deviation from their mean of the pressure values P_i of each load cell profile:

$$\Delta P = \sqrt{\langle (P_i - \overline{P})^2 \rangle}, \tag{2}$$

where the angle brackets symbolise the average for each flow signal. The larger ΔP, the larger is the number of collisions that exerts pressures that are more different from the mean pressure. For this reason, ΔP is an estimate of particles agitation.

We normalise ΔP with respect to the mean pressure:

$$D = \frac{\Delta P}{\overline{P}}. \tag{3}$$

We expect the retarding force (which dissipates the energy of the flow) to be proportional to ΔP through the ground contact surface. Parameter D can be interpreted as the ratio between retarding and driving forces if the mean pressure is proportional to the flow mass (our data show that they are positively correlated) and the driving force is proportional to the mass of the flow (the driving force of a sliding rigid body, for example, is its slope-parallel component of weight). It is the ratio between these forces that determines the mobility of the flows. The larger D (i.e., the larger the normalised particles agitation), the larger is expected to be the relative energy dissipation of the flow in a specific spot (where the load cell is located, for example), and for this reason, D is expected to be proportional to the reciprocal of a potential flow mobility. Table 1 shows the mean values of the quantities used to estimate this parameter. The values of $\overline{P}$ that change more significantly for different flow masses than different grain sizes (Table 1) can support our idea that $\overline{P}$ can be considered mainly a function of the flow mass.

For each load cell signal, we compute also the ratio between the number N of data points with pressure value larger than a given background and the total number T of data points:

$$n = \frac{N}{T}. \tag{4}$$

In each load cell signal, we consider as background the data points with values smaller than the mean pressure (the mean pressure is always very small when compared to the pressure values of the signal peaks).

A different measure of the reciprocal of mobility is

$$\mu_A = \frac{h}{l}, \tag{5}$$

where h is the vertical drop of the centre of mass of the granular material and l is its horizontal distance of travel (Fig. 1). The smaller

the value of μ_A, the larger is the actual flow mobility. This ratio can be considered as an apparent coefficient of friction (Scheidegger, 1973). How different is this estimate of the reciprocal of flow mobility from that provided by parameter D is discussed at the end of the paper. Because we take into account the position of the flows centre of mass at $x=0$, the higher elevations behind the gate of the centres of mass of larger volumes do not affect our evaluation of mobility.

5. Dimensional analysis

Here we consider that the potential flow mobility (determined at the grain scale and expressed as the reciprocal of the normalised particles agitation D) is a function of the following variables: mean grain size δ (Cagnoli and Romano, 2010), volume V of flow or deposit (Scheidegger, 1973), initial (at $x=0$) flow speed s, acceleration of gravity g, density ρ_s of the particles, density ρ_f of the interstitial fluid, dynamic viscosity η of the interstitial fluid, angle of internal friction ϕ of the particles, coefficient of restitution e of the rock material and average height i of the ground surface asperities. This corresponds to the following relationship:

$$D = f_1\left(\delta, V, s, g, \rho_s, \rho_f, \eta, \phi, e, i\right). \tag{6}$$

According to the Buckingham Pi theorem, eleven variables with three fundamental quantities (mass, length and time) can be expressed by a physically meaningful equation with eight dimensionless parameters. Eq. (6) is therefore replaced by

$$D = f_2\left(\frac{\delta}{V^{1/3}}, \quad \frac{\delta g}{s^2}, \quad \frac{\eta}{s\rho_s\delta}, \quad \frac{\delta}{i}, \quad \frac{\rho_f}{\rho_s}, \quad \phi, \quad e\right), \tag{7}$$

which is the relationship between our dependent dimensionless parameter D and the independent dimensionless ones.

The first independent dimensionless parameter represents the normalisation of grain size with respect to volume because a fragment can be considered large or small depending on the size of the volume of the flow or deposit. The numerator (δMg) of the second dimensionless independent parameter is proportional (by means of an apparent friction coefficient describing the interaction between flow and chute surface) to the work carried out by retarding forces on a characteristic mass M along a characteristic distance δ. This distance is considered along the chute even if the trigonometric function to compute the appropriate component of the force is not entered in the scaling parameter. The denominator (Ms^2) of the second independent parameter represents twice the initial kinetic energy of the characteristic mass (here potential energy is not considered because all flows are compared at the same elevation). Therefore, the second dimensionless parameter is the ratio between dissipated energy along a characteristic portion of the chute and the initial kinetic energy.

The third independent dimensionless parameter represents the ratio of the viscous shear stresses to the inertial grain stresses and it corresponds to the reciprocal of the Bagnold number (Bagnold, 1954). The fourth independent parameter represents the relative importance of the size of the ground asperities with respect to the grain size. The fifth parameter is the ratio of fluid density to grain density. Parameters sixth and seventh are the angle of internal friction and the coefficient of restitution, respectively, which are dimensionless variables.

The values of the last three independent dimensionless parameters (ρ_f/ρ_s, ϕ and e) do not vary in our experiments and, for this reason, they are not responsible for the different mobility of our different flows. Here with the coefficient of restitution e we refer to the intrinsic bounciness of the same rock material all our particles are made of. The density of our interstitial fluid (air) is also significantly small ($\rho_f = 1.2$ kg/m^3) when compared with that of the rock fragments. The third parameter varies and because it corresponds to the reciprocal of the Bagnold number we can use the critical value of this well known number to distinguish the different flow regimes. The Bagnold number represents the ratio of inertial grain stresses to viscous shear stresses. In all our flows, this number has values that are significantly larger than the critical threshold equal to 450 indicating that our flows are collision-dominated. This means that the value of air viscosity, $\eta = 1.86\times10^{-5}$ kg/(m sec), is relatively too small for air to affect our particles collisions and, thus, flow mobility. Also the fourth parameter varies but the surface asperities are always the same in our experiments and their effect on our flow mobility is already accounted for by the different grain size values. Here we do not take into consideration prolonged frictional contacts at the base of the flows because the load cell data show that the basal interaction consists of collisions. This corresponds, in our flows, to large values (larger than the critical threshold equal to 0.1) of the Savage number (Savage and Hutter, 1989) indicating that grain collision stresses dominate grain friction stresses. Furthermore, high pore pressures (if any) should dissipate quickly because of the relatively large pore pressure diffusivity that is expected in all our flows that are expanded because of particles collisions (for this reason, pore pressure is not considered in our analysis).

Therefore, we consider the first and second dimensionless independent parameters as those containing the variables whose different values are responsible for the different mobility of our flows. We test the idea that the reciprocal of flow mobility is proportional to a power of grain size because our experiments show that finer grain size flows are more mobile than coarser ones (Cagnoli and Romano, 2010). Here the grain size effect is normalised with respect to the initial speed whose increase does increase the travel distance. We suggest that the mobility increase of flows with finer particles (all the other features equal) is the result of a decrease of particles agitation as grain size decreases. This can be explained considering that with finer grain size (all the other features equal), there is a relatively larger number of particles in the flows and, for this reason, fragments agitation at the contact with the containing boundary surfaces penetrates relatively less inside the flows. Flows with fragments that are less agitated dissipate less energy per unit of travel distance and, therefore, they have longer travel distances (Cagnoli and Romano, 2010). We test also the idea that the reciprocal of flow mobility is inversely proportional to a power of flow volume (here normalised with respect to grain size) because when volume increases, the mass of a particle becomes relatively smaller with respect to the total mass of the flow and, for this reason, particles agitation due to the interaction with the containing boundary surfaces is expected to penetrate relatively less inside the flow. This corresponds to test the validity of an expression where the reciprocal of the potential flow mobility (represented here by D) is proportional to the following scaling parameter:

$$\alpha = \frac{\delta^2 g}{V^{1/3}s^2}, \tag{8}$$

which is the product of the first and second independent parameters of Eq. (7).

Parameter α represents the ratio of dissipated energy along a characteristic portion of the chute to twice the initial kinetic energy (i.e., the meaning of the second independent parameter) divided by the reciprocal of the first independent parameter that is proportional to the number of particles in the flow because it corresponds to V/δ^3 (where volume V is, more appropriately, that of the total solid mass of the flow). Therefore, considering the characteristic mass M equal to that of a single grain, parameter α represents the ratio of the average energy dissipated to move each grain past one another in a single point along the slope (because the characteristic length is δ) to twice the kinetic energy of the entire solid mass of the flow. The rationale of this parameter is that, as far as the energy dissipation is concerned, it is the relative amount of more agitated particles with respect to the total number of particles that is important. The grain size is considered the characteristic length because we are dealing with

the agitation of the rock fragments (parameter D) in one single point along the chute (where the load cell is located). Flow depth and flow length are inappropriate because our flows are not fluids with a basal hydrostatic pressure and only a small portion of the flow length affects the load cell at any moment in time. In other words, as far as the stresses-generating grain-scale mechanics is concerned, the pertinent length scale is that of the grain size (Iverson, 1997).

In our calculations, we use the volume of the deposits instead of that of the flows because more appropriate to approximate that of the total solid mass if the solid volume fraction can be assumed approximately the same in all deposits (in our case, data fall on a single fitting curve with both volumes). This is certainly not true with the volume of expanded travelling flows of colliding particles. If different flows are considered along the same small portion of the chute (where the load cell is located for example), a comparison between their values of α does not require the introduction at its numerator of the trigonometric function to compute the appropriate component of the force. Parameter α can be applied also to granular material that starts from rest because it is always possible to consider the initial deformation of a mountain slope or volcanic dome as a distinct phenomenon positioning $x=0$ in a more distal location (Fig. 1) where s is different from zero and, for this reason, it can be inserted at the denominator of α. Table 2 shows the averages of the quantities used to estimate this parameter.

6. Particle image velocimetry analysis

The high-speed movies are analysed by particle image velocimetry (PIV) technique (Pudasaini and Hutter, 2006; Raffel et al., 2007). This technique allows estimates of the longitudinal and transversal velocity components of the particles on the surface of the travelling flows. Our PIV analysis is performed here as described by Cagnoli and Romano (2010) dividing the image into a regular grid of interrogation windows that are 12×12 pixels in size and computing cross-correlation between image pairs separated by 1/1000 s. Our algorithm uses advanced image processing techniques such as window-offset, sub-pixel accuracy and image deformation (Di Florio et al., 2002). Window overlapping is here equal to 75% and, as sampling rate, we skip one frame every two in the movie sequence.

We compute the normalised average squared deviation from their mean ($\bar{u}$) of the particles transversal (with respect to flow direction) speeds u_i:

$$A = \frac{\left\langle (u_i - \bar{u})^2 \right\rangle}{s^2}, \tag{9}$$

where the angle brackets symbolise the average (Cagnoli and Romano, 2010). To enable comparisons between different experiments, the average squared deviation of the transversal speed is estimated in a central area of all flows when it is centred at 8 cm from $x=0$ down the chute. In this location, all flows have already their mature shape of travel and this central area is narrow enough to exclude the more agitated fragments in contact with the containing lateral surfaces. The central area consists of 7 contiguous rows of interrogation windows.

Table 2
Mean volume (cm^3) of deposits and mean initial flow speed (m/s) versus mean grain size (mm) and initial granular mass (g). The uncertainties are the error of the mean (i.e., the square root of the variance divided by the number of measurements).

	2.5 mm	1.5 mm	0.75 mm	
30 g	0.93 ± 0.02 m/s	0.95 ± 0.02 m/s	1.00 ± 0.01 m/s	21.153 ± 0.255 cm^3
15 g	0.88 ± 0.02 m/s	0.88 ± 0.02 m/s	0.98 ± 0.01 m/s	9.929 ± 0.260 cm^3
5 g	0.89 ± 0.02 m/s	0.89 ± 0.01 m/s	0.93 ± 0.01 m/s	3.060 ± 0.182 cm^3

Table 3
Average squared deviation from their mean of the particles speeds in the transversal direction $(m/s)^2$ versus mean grain size (mm) and initial granular mass (g). The uncertainties are the error of the mean (i.e., the square root of the variance divided by the number of measurements).

	2.5 mm	1.5 mm	0.75 mm
30 g	0.0068 ± 0.0001 $(m/s)^2$	0.0048 ± 0.0002 $(m/s)^2$	0.0031 ± 0.0002 $(m/s)^2$
15 g	0.0084 ± 0.0002 $(m/s)^2$	0.0057 ± 0.0001 $(m/s)^2$	0.0040 ± 0.0001 $(m/s)^2$
5 g	0.0093 ± 0.0004 $(m/s)^2$	0.0079 ± 0.0004 $(m/s)^2$	0.0046 ± 0.0003 $(m/s)^2$

The numerator of parameter A is the transversal velocity fluctuation and it is meant to represent the agitation of the particles due to the interaction with the containing surfaces. The normalisation is performed with respect to the initial flow speed s because the longitudinal velocity of the flows can affect the agitation of the particles. Therefore, parameter A is the agitation of the particles due to the interaction with the containing surfaces per unit of longitudinal speed (Cagnoli and Romano, 2010). The numerator of A represents twice the kinetic energy per unit of mass in the transversal direction (because $\bar{u}$ is virtually zero in all flows, as expected in symmetrical channels) whereas the denominator represents that in the longitudinal direction. Because, as far as mobility is concerned, the most efficient flows are those which spend all their kinetic energy in the downhill direction, the larger A, the smaller is expected to be flow mobility (Cagnoli and Romano, 2010). Tables 3 and 2 show the averages of the quantities used to estimate parameter A.

7. Results: basal pressures and flow mobility

Load cell profiles (Fig. 4) show that the basal pressure changes irregularly with time presenting signal peaks separated by zero-pressure data points. The magnitude of these signal peaks can be significantly large and they produce meaningful trends. We interpret them to be the results of collisions of particles and or clusters of particles. Fig. 4 shows also that volume affects the length of the flow signal. The larger the volume, the longer the flow signal because the longer is the flow.

The maximum signal pressures (that can be almost 30,000 Pa) are significantly larger than the mean pressures (always below 150 Pa) as visible in Figs. 5 and 6. The larger the grain size, the larger is the maximum pressure (Fig. 5). The ranges of maxima of the 30 and 5 g tests overlap but the 5 g tests tend to have smaller values. The mean pressures are larger for larger volumes and for larger grain sizes, even if the differences due to our different grain sizes are not much larger than the scatter of values produced by the experiments with the same characteristics (Fig. 6).

Fig. 7 shows that the relative portion of flow signal that is above background (i.e., the portion consisting of signal peaks) increases as parameter α decreases (i.e., as grain size decreases and volume increases). Fig. 8 shows that the normalised particles agitation D increases as parameter α increases (i.e., as grain size increases and volume decreases). In Fig. 8, data are well fitted by a straight line. The fact that data in Fig. 8 fall along a single curve confirms that α considers all the variables that are relevant in our experiments.

Fig. 9 illustrates the values of the apparent coefficient of friction μ_A that is plotted versus α. The figure clearly shows that the actual flow mobility increases as grain size decreases (and this is true for the three flow masses). However, the difference between the mobility of the flows with same grain size but different volume is not visible. In Figs. 6–9, the five experiments with identical characteristics generate similar results suggesting good experimental repeatability.

Examples of the velocities (obtained by PIV analysis) of the particles on the surface of the flows are shown in Fig. 10. Figs. 10A and 10B illustrate flows with different grain sizes but the same volume. In Fig. 11, normalised agitation A is plotted versus the apparent coefficient

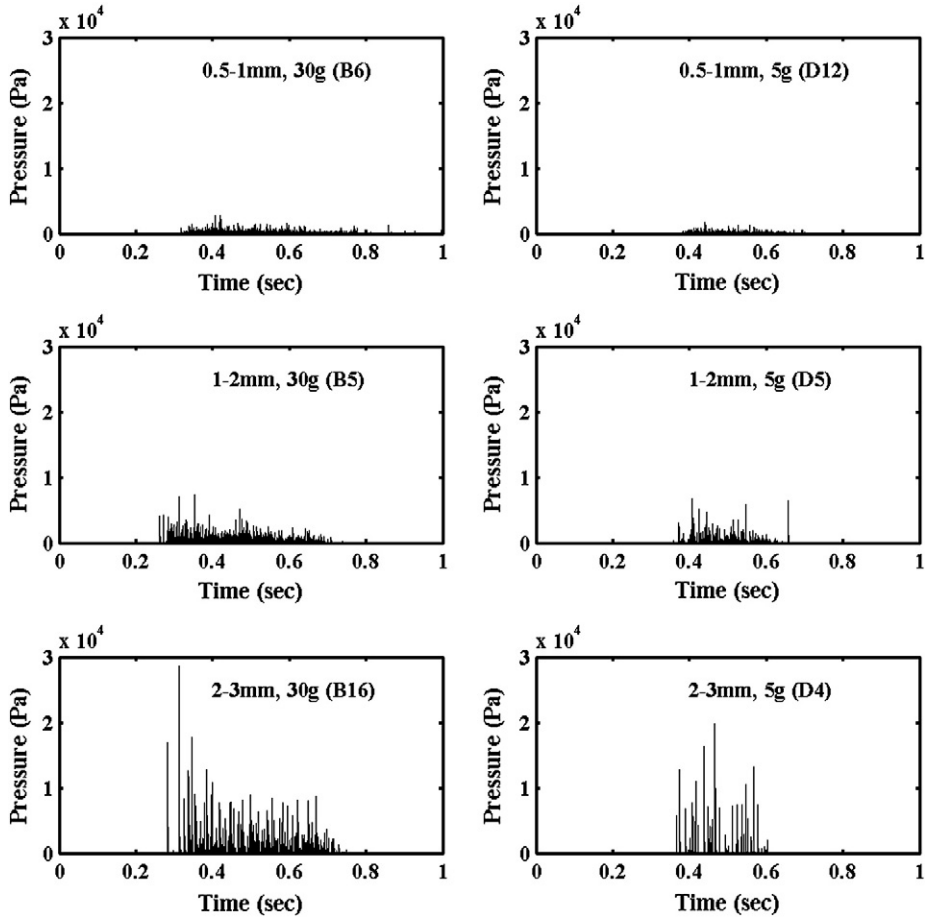

Fig. 4. Examples of load cell signals generated by flows with different grain sizes (the values in millimetres) and different initial granular masses (the values in grams).

of friction μ_A. In this figure, the agitation decreases as grain size decreases and as flow volume increases.

Finally, to test the meaning of parameters D and A, we plot in Fig. 12 the mean values of these parameters for the three grain sizes of the 30 and 5 g flows. Fig. 12 shows that these parameters have a positive correlation suggesting that they represent the same normalised particles agitation. This is consistent with our interpretation of parameter D as an estimate of the relative energy dissipation of the flows (because the larger the agitation, the larger the dissipation) and, for this reason, parameter D can be considered proportional to the reciprocal of a potential (because it is measured locally) flow mobility. That these parameters are correlated (irrespective of the fact that one is measured at the top and the other at the base of the flows) is not surprising because particles agitation, within the flows, propagates inward and upward from the boundary surfaces. Thus, a flow that is more agitated at the top is more agitated also in its interior. Therefore the fitting straight line in Fig. 8 is consistent with a proportionality between the reciprocal of a potential flow mobility and parameter α.

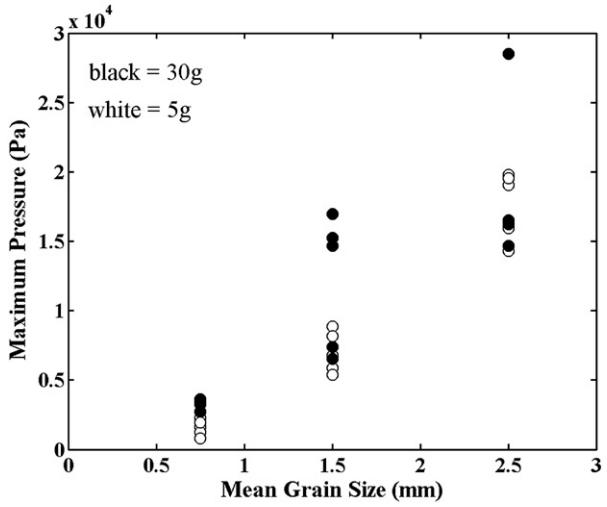

Fig. 5. Pressure values of the largest peak of the load cell signals.

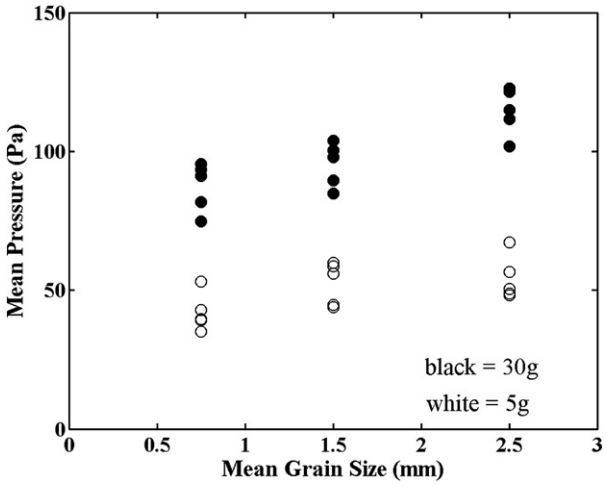

Fig. 6. Mean pressures exerted on the load cell by the flows during their time of transit.

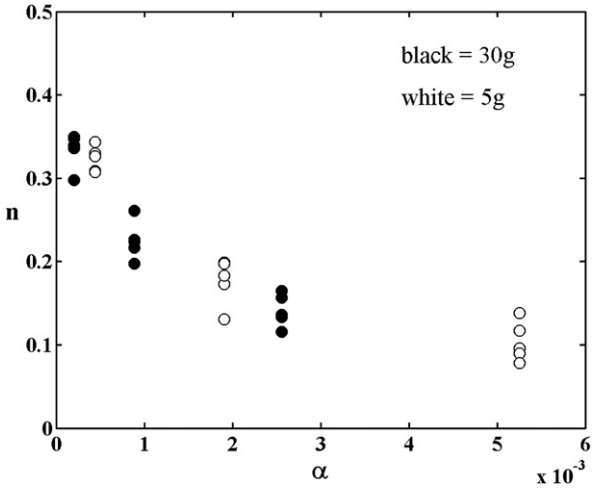

Fig. 7. Parameter n represents the ratio between the number of data points with values larger than background and the total number of data points in the load cell signal generated during the flow transit on the load cell. Parameter α is a normalised grain size with respect to volume of granular mass and initial speed. Mean α values for each group of experiments with identical characteristics are shown here.

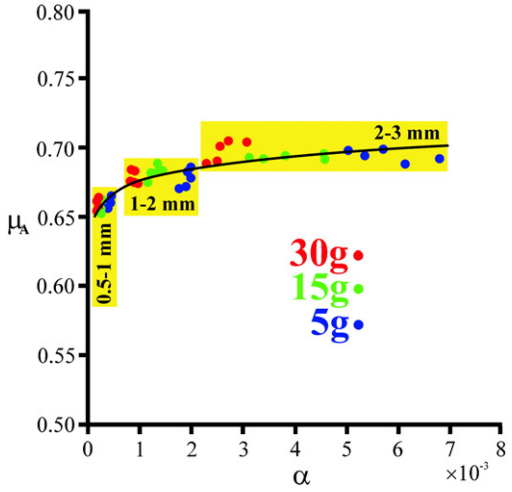

Fig. 9. Apparent coefficient of friction μ_A versus parameter α which is a normalised grain size with respect to volume of granular mass and initial speed. The values in millimetres are the grain size ranges and those in grams the initial granular masses.

8. Discussion

8.1. Basal collisions

The load cell signals show that the interaction of the dry flows with the chute surface is dominated by collisions (Fig. 4). This is certainly true because the maximum pressures (Fig. 5) are much larger than even the static pressure at the base of a body with bulk density equal to that of our rock fragments and the largest flow thickness (~1 cm). Such a variable basal pressure suggests that the use of Coulomb's law when modelling these flows can only refer to a time-averaged value of pressure instead of the actual one that varies significantly during flow motion and that can be equal to zero from time to time. Coulomb's law refers to a sliding rigid body whose contact with the ground surface is continuous in time so that the basal pressure is always different from zero. Although it is always possible to measure an average shear stress and an average normal stress, and thus, it is always possible to generate a Coulomb's law (where the friction coefficient is equal to the ratio, whatever its value, between these two stresses), our experiments demonstrate that the interaction between flows and containing boundary surfaces is different from sliding. It is for this reason that we use a normalised particles agitation (parameter D) as an estimate of the reciprocal of the potential (i.e., measured locally) flow mobility in the dimensional analysis. Because the values of D are expected to change at different slope angles, it is important to compare those of different flows when measured in the same place.

Granular mass flows can present a plug that travels above a basal layer of colliding particles (Anderson and Jackson, 1992; Cagnoli and Manga, 2004). We do expect that the plug can oscillate impacting the ground surface from time to time (Cagnoli and Quareni, 2009). The

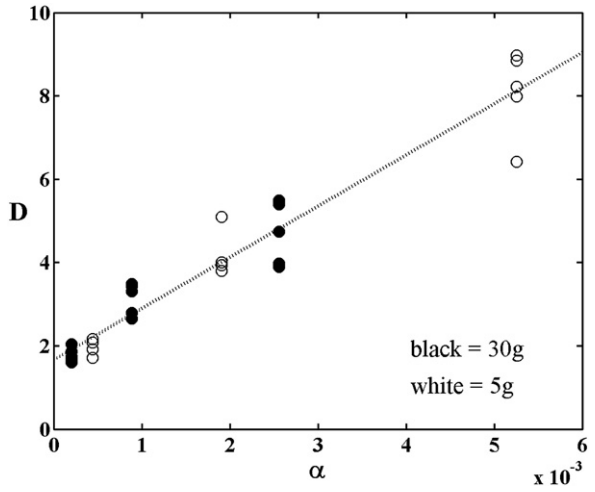

Fig. 8. Parameter D is a normalised particles agitation. Parameter α is a normalised grain size with respect to volume of granular mass and initial speed. The curve fitting the data is a straight line. Mean α values for each group of experiments with identical characteristics are shown here.

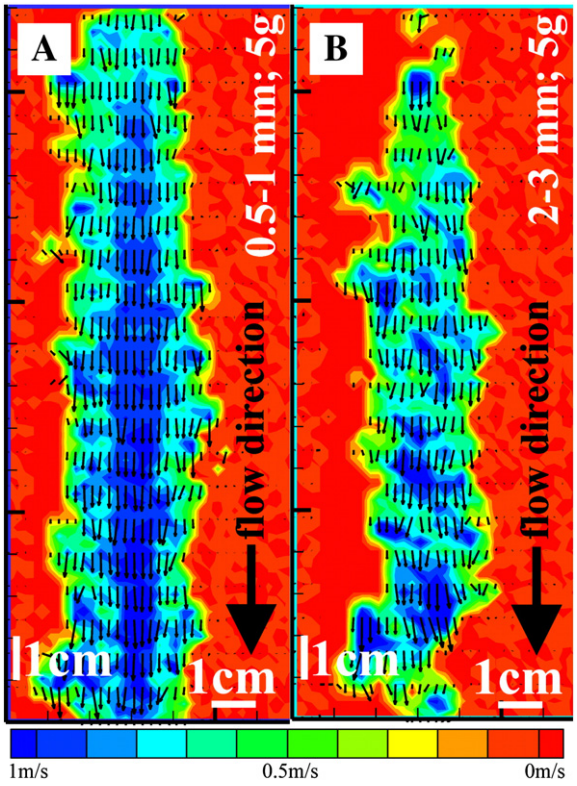

Fig. 10. Velocity fields of the particles on the surface of two flows with the same mass (the values in grams) but different grain size (the values in millimetres) as obtained by particle image velocimetry analysis. The small arrows are instantaneous velocity vectors. The centres of these flows are located at 8 cm from x = 0 down the chute.

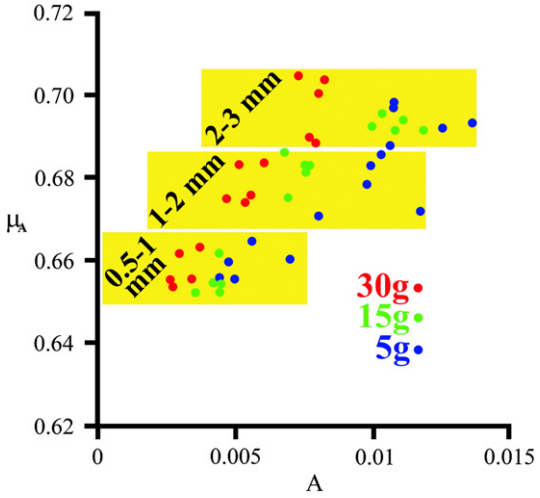

Fig. 11. Apparent coefficient of friction μ_A versus agitation A. The values in millimetres are the grain size ranges and those in grams are the initial granular masses.

question is whether the collisions that are visible in our load cell signals (Fig. 4) are only due to single fragments (such as those of the basal layer) or they are also due to portions of the plug transiting on the load cell and impacting its plate. It is important to realize that because most of the flow mass is spread along the relatively long length of the flow, only a portion of the plug (and thus of the total flow mass) can collide with the chute surface in each place and at any time.

8.2. Load cell data

The maximum pressures of Fig. 5 are affected by both the mass and the impact velocity of the particles. Maximum pressure increases as grain size increases because the larger the mass of the fragment, the larger is the force exerted during the collision. However, data are scattered because the impact velocity has probably a distribution of different values in each flow. The larger values of the maximum pressures in Fig. 5, for example, can be explained by a combination of relatively large impact velocities and large masses. We wonder whether the fact that the 30 g tests tend to have maxima that are larger than those of the 5 g tests confirms that the collisions are also due to larger clusters of fragments (such as portions of thicker plugs).

The increase of the mean basal pressure as grain size increases (Fig. 6) can again be explained considering that fragments with larger masses exert larger forces when colliding. The increase of mean pressure at larger volume, on the other hand, could be due to a larger number of collisions per unit of time (because there are more particles in larger volumes) but it could also be due to thicker plugs or larger clusters of fragments impacting the basal surface.

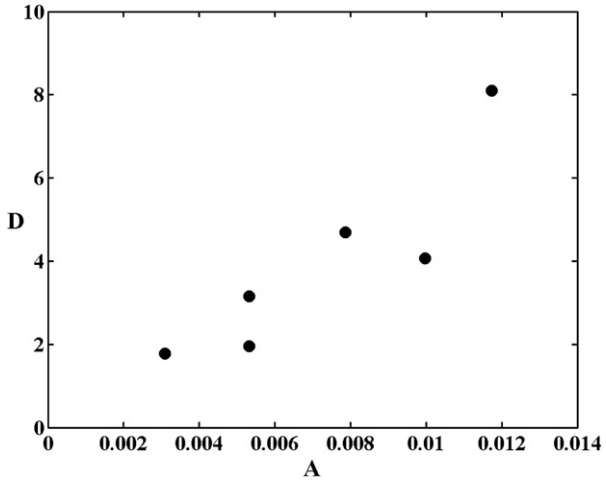

Fig. 12. Plot of the mean values of parameters D and A for the three grain sizes of the 30 and 5 g flows.

According to Fig. 7, the portion of signal above background increases as volume increases and as grain size decreases. This trend can be explained by the increase of the number of collisions per unit of time due to a relatively larger number of particles when (all the other things equal) the volume increases or the grain size decreases. When the grain size increases, there are only slightly larger mean pressures (Fig. 6) because even if the collisions exert on average larger forces (Fig. 5), there are fewer collisions (Fig. 7).

Fig. 8 shows that parameter D increases as grain size increases and as flow volume decreases. Therefore if D represents the energy dissipation in one spot (i.e., the reciprocal of a potential flow mobility), the larger the grain size and the smaller the volumes, the smaller is expected to be the travel distance. This relationship between flow mobility and grain size is confirmed by a previous set of experiments (Cagnoli and Romano, 2010) as well as by the results presented here (Fig. 9). The relationship between flow mobility and volume, on the other hand, is consistent with field observations (Scheidegger, 1973). Moreover, Fig. 8 is consistent also with the expected effect of larger initial velocities that is to produce larger travel distances because the initial energy of the flows is larger.

Data in Fig. 8 collapse along a single straight line confirming that no other variable that affects the energy dissipation has significantly different values in our experiments. This for example confirms that the interstitial fluid does not have a different effect in our different flows. The variables that enter parameter α, on the other hand, have significantly different values (i.e., they are those responsible for the different mobility of our flows). The intercept between this straight line and the vertical axis in a position different from the origin can be understood considering that even if α tends to zero, the energy dissipation decreases but it must always be different from zero (i.e., there is always a larger than zero energy dissipation also at very small α values).

8.3. Flow mobility

We explain the mobility increase of flows with finer particles (all the other features equal) as the result of a decrease of particles agitation (and thus of energy dissipation) as grain size decreases (Cagnoli and Romano, 2010). For example, Fig. 10 confirms that the magnitude of the particles velocities is more variable (i.e. the particles are more agitated) in the flow with coarser grain size than in the flow with finer grain size. Volume is expected to have an effect on flow mobility that is the opposite of that of grain size because when volume increases, the mass of a particle becomes relatively smaller with respect to the total mass of the flow. In this case, particles agitation due to the interaction with the containing boundary surfaces is expected to penetrate relatively less inside the flow and, for this reason, it is expected to affect a relatively smaller portion of the total mass of the flow. Fig. 11 confirms that agitation A decreases not only when grain size decreases but also when flow volume increases.

In our experiments, our selection of grain sizes and flow volumes is meant to produce a range of flows with different interactions between particles. Flows with the largest volume and smallest grain size have higher densities (Fig. 3A), whereas flows with the smallest volume and largest grain size have significantly more dispersed particles (Fig. 3B). The other flows plot in between as far as flow density is concerned. We expect the formation of plugs to occur in flows with relatively finer grain size and larger volume (Figs. 3A and 10A) whereas flows with relatively larger grain size and smaller volume do not present plugs (Figs. 3B and 10B).

Both parameter D and parameter μ_A are meant to represent the reciprocal of flow mobility. The question is then why the measurements of μ_A do not show a different mobility due to the different

volumes (Fig. 9). One possible explanation is that there is a threshold value above which volume affects mobility and that our volumes are smaller than this value. But if this were true, there would be no scaling parameter that takes into account the effect of volume. It is, in any case, true that it is only the cube root of volume that enters parameter α and, for this reason, the effects of the changes of volume are small. For example, doubling the volume has a smaller effect on flow mobility than doubling the grain size. This could explain why in the field only avalanches with huge volumes are seen to be particularly mobile. Moreover, according to Fig. 8, no threshold should exist (unless parameter D is not related to the reciprocal of flow mobility).

If D is related to the reciprocal of flow mobility, the lack of visibility of the volume effect in Fig. 9 could be due to uncertainties when assessing the position of the centre of mass at $x=0$ as well as the position of the centre of mass of the deposit. The identification of the position of this second centre of mass depends, for example, on the identification of the deposit of the flow proper. This deposit is always followed by a distal distribution of individual fragments. Doubts when locating the boundary between deposit and distal distribution increase as grain size increases and flow volume decreases. Thus, an increased overestimate of the distal reach of the volume of deposits with smaller volumes at increasing grain size could explain the downward concave shape of the fitting curve in the plot with μ_A (Fig. 9). This curve is different from the straight line fitting the 30 g flows (whose larger volume makes the uncertainties on the positions of their centres of mass significantly smaller) not only in Fig. 8, but also when μ_A is estimated considering the distance from the centres of mass behind the gate to the centres of mass of the deposits (Cagnoli and Romano, 2010).

There is, however, also an important phenomenon that can affect the effect of volume on the position of the centre of mass of the deposits. Because the most distal part of a flow reaches the less-steep portion of a curved chute and stops before the rear part, rear granular material is prevented from moving further and accumulates behind the already deposited frontal portion. This results in a less distal location of the rear portion of the deposit and, therefore, of its centre of mass. In larger volume flows (that are also longer) this phenomenon is more prominent and it can counteract the larger potential mobility of their centres of mass. This phenomenon is important to consider because it can occur also in nature. Therefore, parameter D represents the reciprocal of the potential (i.e., measured locally and upslope with respect to the deposit) flow mobility, whereas μ_A represents the reciprocal of the actual flow mobility. Parameter D provides information on the intrinsic ability of the flow to dissipate more or less energy in a single spot (the load cell location for example), whereas μ_A considers the entire travel distance and, thus, also other effects such as those due to the slope shape.

9. Conclusions

Parameter α is a scaling parameter that includes three key variables that are expected to affect flow mobility. These variables are grain size, flow volume and initial speed. Our analysis suggests that as grain size decreases and as flow volume increases, the relative energy dissipation decreases and flow mobility is expected to increase. Larger travel distances are, of course, generated also by larger initial speeds. The relationship between grain size and mobility has been confirmed by laboratory experiments (Cagnoli and Romano, 2010) whereas that between volume and mobility is consistent with field observations (Scheidegger, 1973). However, the centres of mass of our larger volume deposits are not located in more distal positions. This could be due to the fact that larger volume flows are also longer and their already deposited frontal part (on a less-steep more-distal position of the slope) prevents the rear granular material and the centre of mass of the flows to move further downhill. The understanding of the variables that affect flow motion is important when assessing natural hazards in mountain regions.

Acknowledgments

We are grateful to Enzo Boschi and Antonio Piersanti for their support. Many thanks to Domenico Pietrogiacomi for his assistance in the laboratory. We are indebted to Giovanni Romeo, Giuseppe Di Stefano and Paolo Benedetti whose electronic engineering skills made the use of the load cell possible. Many thanks also to P. Bartelt and an anonymous reviewer for their useful comments.

References

Anderson, K.G., Jackson, R., 1992. A comparison of the solutions of some proposed equations of motion of granular materials for fully developed flow down inclined planes. J. Fluid Mech. 241, 145–168.
Bagnold, R.A., 1954. Experiments on a gravity-free dispersion of large solid spheres in a Newtonian fluid under shear. Proc. R. Soc. London 225, 49–63.
Bartelt, P., Buser, O., Platzer, K., 2007. Starving avalanches: frictional mechanisms at the tails of finite-sized mass movements. Geophys. Res. Lett. 34, L20407. doi:10.1029/2007GL031352.
Becker, G.F., 1905. A feature of Mayon Volcano. Proc. Wash. Acad. Sci. VII, 277–282.
Berti, M., Genevois, R., LaHusen, R., Simoni, A., Tecca, P.R., 2000. Debris flow monitoring in the Acquabona watershed on the Dolomites (Italian Alps). Phys. Chem. Earth B 25, 707–715.
Cagnoli, B., Manga, M., 2004. Granular mass flows and Coulomb's friction in shear cell experiments: implications for geophysical flows. J. Geophys. Res. 109, F04005. doi:10:1029/2004JF000177.
Cagnoli, B., Quareni, F., 2009. Oscillation-induced mobility of flows of rock fragments with quasi-rigid plugs in rectangular channels with frictional walls: a hypothesis. Eng. Geol. 103, 23–32.
Cagnoli, B., Romano, G.P., 2010. Effect of grain size on mobility of dry granular flows of angular rock fragments: an experimental determination. J. Volcanol. Geotherm. Res. 193, 18–24. doi:10.1016/j.jvolgeores.2010.03.003.
Di Florio, D., Di Felice, F., Romano, G.P., 2002. Windowing, re-shaping and re-orientation interrogation windows in particle image velocimetry for the investigation of shear flows. Meas. Sci. Technol. 13 (7), 953–962.
Holtz, R.D., Kovacs, W.D., 1981. An Introduction to Geotechnical Engineering. Prentice-Hall, New Jersey.
Iverson, R.M., 1997. The physics of debris flows. Rev. Geophys. 35, 245–296.
Johnson, A.M., Rodine, J.R., 1984. Debris flow. In: Brunsden, D., Prior, D.B. (Eds.), Slope Instability. John Wiley and Sons, New York, pp. 257–361.
Lambe, T.W., Whitman, R.V., 1969. Soil Mechanics. John Wiley and Sons, New York.
Mangeney, A., Bouchut, F., Thomas, N., Vilotte, J.P., Bristeau, M.O., 2007. Numerical modeling of self-channeling granular flows and of their levee-channel deposits. J. Geophys. Res. 112, F02017. doi:10.1029/2006JF000469.
McArdell, B., Bartelt, P., Kowalski, J., 2007. Field observations of basal forces and fluid pore pressure in a debris flow. Geophys. Res. Lett. 34, L07406. doi:10.1029/2006GL029183.
Pudasaini, S.P., Hutter, K., 2006. Avalanche Dynamics. Springer, Berlin.
Raffel, M., Willert, C.E., Wereley, S.T., Kompenhans, J., 2007. Particle Image Velocimetry. Springer, Berlin.
Savage, S.B., Hutter, K., 1989. The motion of a finite mass of granular material down a rough incline. J. Fluid Mech. 199, 177–215.
Scheidegger, A.E., 1973. On the prediction of the reach and velocity of catastrophic landslides. Rock Mech. 5, 231–236.
Schmincke, H.-U., 2004. Volcanism. Springer, Berlin.
Sheridan, M.F., Stinton, A.J., Patra, A., Pitman, E.B., Bauer, A., Nichita, C.C., 2005. Evaluating Titan2D mass-flow model using the 1963 Little Tahoma Peak avalanches, Mount Rainier, Washington. J. Volcanol. Geotherm. Res. 139, 89–102.
Zenz, F.A., Othmer, D.F., 1960. Fluidization and Fluid-Particle Systems. Reinhold, New York.